

*promoting access to White Rose research papers*



**Universities of Leeds, Sheffield and York**  
**<http://eprints.whiterose.ac.uk/>**

---

This is an author produced version of a paper published in **Monthly Notices of the Royal Astronomical Society**.

White Rose Research Online URL for this paper:  
<http://eprints.whiterose.ac.uk/8905/>

---

**Published paper**

Bushby, P.J., Houghton, S.M., Proctor, M.R.E. and Weiss, N.O. (2008)  
*Convective intensification of magnetic fields in the quiet Sun*. Monthly Notices of the Royal Astronomical Society, 387 (2). pp. 698-706.

<http://dx.doi.org/10.1111/j.1365-2966.2008.13276.x>

---

# Convective intensification of magnetic fields in the quiet Sun

P.J.Bushby<sup>1\*</sup>, S.M.Houghton<sup>2</sup>, M.R.E.Proctor<sup>3</sup> and N.O.Weiss<sup>3</sup>

<sup>1</sup>*School of Mathematics and Statistics, Newcastle University, Newcastle upon Tyne NE1 7RU, UK*

<sup>2</sup>*Department of Applied Mathematics, University of Leeds, Leeds LS2 9JT, UK*

<sup>3</sup>*DAMTP, Centre for Mathematical Sciences, University of Cambridge, Wilberforce Road, Cambridge CB3 0WA, UK*

Submitted ??/??/08

## ABSTRACT

Kilogauss-strength magnetic fields are often observed in intergranular lanes at the photosphere in the quiet Sun. Such fields are stronger than the equipartition field  $B_e$ , corresponding to a magnetic energy density that matches the kinetic energy density of photospheric convection, and comparable with the field  $B_p$  that exerts a magnetic pressure equal to the ambient gas pressure. We present an idealised numerical model of three-dimensional compressible magnetoconvection at the photosphere, for a range of values of the magnetic Reynolds number. In the absence of a magnetic field, the convection is highly supercritical and is characterised by a pattern of vigorous, time-dependent, “granular” motions. When a weak magnetic field is imposed upon the convection, magnetic flux is swept into the convective downflows where it forms localised concentrations. Unless this process is significantly inhibited by magnetic diffusion, the resulting fields are often much greater than  $B_e$ , and the high magnetic pressure in these flux elements leads to their being partially evacuated. Some of these flux elements contain ultra-intense magnetic fields that are significantly greater than  $B_p$ . Such fields are contained by a combination of the thermal pressure of the gas and the dynamic pressure of the convective motion, and they are constantly evolving. These ultra-intense fields develop owing to nonlinear interactions between magnetic fields and convection; they cannot be explained in terms of “convective collapse” within a thin flux tube that remains in overall pressure equilibrium with its surroundings.

**Key words:** convection – (magnetohydrodynamics:) MHD – Sun: granulation – Sun: magnetic fields – Sun: photosphere

## 1 INTRODUCTION

High resolution observations of the solar photosphere have greatly enhanced our understanding of the complex interactions between magnetic fields and turbulent convective motions. Modern ground-based telescopes, such as the SST on La Palma, and space-borne instruments, such as the Solar Optical Telescope (SOT) on the recently-launched Hinode satellite, can now resolve the fine structure of photospheric magnetic fields. Such high resolution observations have already provided new insights into the magnetic field structures that can be found in sunspot penumbrae (Scharmer et al. 2002), plage regions (Berger et al. 2004) and the quiet Sun (see, for example, Centeno et al. 2007; Rezaei et al. 2007). In the quiet Sun, localised concentrations of intense vertical magnetic flux often accumulate in the convective downflows (Lin & Rimmele 1999; Domínguez Cerdeña, Kneer &

Sánchez Almeida 2003; Centeno et al. 2007). These localised flux concentrations typically show up as bright points in G-band images of the photospheric granulation (see, for example, Berger & Title 1996, 2001). Direct measurements indicate that the peak field strength within these small-scale magnetic features is often well in excess of a kilogauss (see, for example, Grossmann-Doerth, Keller & Schüssler 1996; Domínguez Cerdeña et al. 2003). Although kilogauss-strength magnetic features occupy only a small fraction of the quiet solar surface, these localised flux concentrations contain a significant proportion of the total (unsigned) quiet Sun magnetic flux (Domínguez Cerdeña, Sánchez Almeida & Kneer 2006; Sánchez Almeida 2007).

The origin of quiet Sun magnetic fields remains an open question. Either these magnetic fields are generated locally at the photosphere, as the result of small-scale convectively-driven dynamo action (Cattaneo 1999; Cattaneo & Hughes 2006; Vögler & Schüssler 2007), or they were originally generated elsewhere in the solar interior and are simply being

\* E-mail: paul.bushby@ncl.ac.uk (PJB)

re-processed and amplified by the local convective motions. What is clear, however, is that the granular convective upwellings at the solar photosphere will tend to expel magnetic flux, causing it to accumulate in the convective downflows (Proctor & Weiss 1982). This explains the observed association between quiet Sun magnetic fields and the intergranular lanes. However, the peak field strength that is measured in these regions is more difficult to explain. Estimates of the kinetic energy density of the granular convection in the solar photosphere suggest that magnetic field strengths greater than approximately 400G would exceed the “equipartition” value,  $B_e$ , at which the magnetic energy density of these localised fields is comparable to the granular convective kinetic energy density (see, for example, Galloway, Proctor & Weiss 1977). Since the magnetic energy density is proportional to the square of the magnetic field strength, the observed kilogauss-strength fields in the quiet Sun have a magnetic energy density that is an order of magnitude larger than equipartition. In fact, a better estimate for the observed field strengths is given by  $B_p$ , which corresponds to the field strength at which the local magnetic pressure balances the ambient granular gas pressure.

In theoretical studies of Boussinesq magnetoconvection (see e.g. Galloway et al. 1977; Galloway, Proctor & Weiss 1978; Galloway & Moore 1979), the process of magnetic flux expulsion leads naturally to the formation of localised flux concentrations at the edges of convective cells. For axisymmetric converging flows, the *kinematic* flux concentration of weak magnetic fields produces peak fields that scale linearly with the magnetic Reynolds number,  $Rm$ , whilst the width of the resulting magnetic feature is proportional to  $Rm^{-1/2}$ . However, for stronger fields this amplification process is limited by *dynamical* effects. Since the magnetic pressure does not play a role in Boussinesq magnetoconvection, any magnetic feedback is due to the non-conservative component of the Lorentz force, which results from the magnetic curvature. In the dynamical regime, the peak field can only exceed  $B_e$  for large values of the magnetic Prandtl number (the ratio of the kinematic viscosity of the fluid to its magnetic diffusivity). Formally, this scaling can only be verified for small Reynolds numbers,  $Re$ , although it appears not to be restricted to this parameter regime (Cattaneo 1999). Kerswell & Childress (1992) also found a similar magnetic Prandtl number dependence in their idealised boundary-layer study of the equilibrium of a thin flux tube in steady compressible convection (see also Cameron & Galloway 2005). Unfortunately, estimates of the magnetic Prandtl number in the solar photosphere indicate that this diffusivity ratio is extremely small (see, for example, Ossendrijver 2003). So although these comparatively idealised models can explain the formation of highly localised magnetic features at large  $Rm$ , they are unable to account for the appearance of super-equipartition, kilogauss-strength magnetic fields in the quiet Sun.

Since the peak magnetic field in kilogauss-strength magnetic features is comparable to  $B_p$ , the magnetic pressure is bound to play a significant role in the local dynamics. If a magnetic feature is assumed to be in pressure balance with its non-magnetic surroundings, the internal gas pressure must be smaller than that of the surrounding fluid in order to compensate for the large magnetic pressure. Unless these features are much cooler than their surroundings,

this reduction in gas pressure is most easily achieved if these magnetic regions are at least partially evacuated (see, for example, Proctor 1983; Proctor & Weiss 1984). This effect is absent from Boussinesq models, which neglect the effects of compressibility, so it is inevitable that such models underestimate the peak fields that can be generated by the process of flux concentration at the solar photosphere. When seeking to explain the formation of kilogauss-strength magnetic fields in the quiet Sun, it is therefore important to consider the effects of compressibility (see e.g. Hughes & Proctor 1988).

The most widely studied compressible model of magnetic field amplification in the quiet Sun is the “convective collapse” instability of thin magnetic flux tubes (Webb & Roberts 1978; Spruit 1979; Spruit & Zweibel 1979; Unno & Ando 1979). Convective collapse models consider the linear stability of a thin vertical magnetic flux tube embedded in a non-magnetic, superadiabatically stratified atmosphere. There are initially no convective motions along the tube, which is assumed to be in pressure balance with its surroundings. Provided that the initial magnetic field is not too strong, the flux tube is subject to a convective instability that drains plasma vertically out of the tube. As the plasma drains out of the tube, the local pressure balance implies that the tube must “collapse” to form a narrower (and therefore more intense) magnetic flux concentration. This instability will continue to operate until the magnetic field is strong enough to suppress convective motions. This model certainly represents a plausible mechanism for the formation of kilogauss-strength magnetic fields (the only restriction being that the peak field,  $B_{max} \leq B_p$ ). Having said that, this model has its limitations (Hughes & Proctor 1988; Thomas & Weiss 1992, 2008). In particular, the thin flux tube approximation does not appear to be consistent with photospheric observations (see, e.g. Berger & Title 1996; Berger et al. 2004): even in the quiet Sun, the observed magnetic regions seem to form a constantly-evolving “magnetic fluid” (see, for example, Thomas & Weiss 2008), and so cannot simply be regarded as a collection of discrete collapsed flux tubes. In addition, the static equilibrium for the instability is rarely achievable in photospheric magnetoconvection. Finally, by reducing the horizontal component of the momentum equation to a simple pressure balance, the model not only ignores the possible dynamical influence of the surrounding convective motions, but also neglects the possible effects of magnetic curvature, which may play an important role in ensuring the equilibrium of more extensive magnetic features (see, for example, Vögler et al. 2005, where curvature effects help to support a peak field,  $B_{max}$ , in excess of  $B_p$ ).

More realistic models of this process can only be studied by carrying out large-scale numerical simulations of convective magnetic flux intensification. In order to make detailed comparisons between numerical simulations and spectral observations, it is necessary to take account of effects such as partial ionisation and radiative transfer (see, e.g., Vögler et al. 2005). This approach has successfully simulated magnetic fields and spectral features that are similar to those observed in plages (Vögler et al. 2005), in sunspot umbrae (Schüssler & Vögler 2006), and in the quiet Sun (Grossmann-Doerth, Schüssler & Steiner 1998; Khomenko et al. 2005; Stein & Nordlund 2006). More idealised models of photospheric magnetoconvection focus entirely upon the interactions between

compressible convection and magnetic fields (e.g. Hurlburt & Toomre 1988; Matthews, Proctor & Weiss 1995; Weiss et al. 1996; Rucklidge et al. 2000; Weiss, Proctor & Brownjohn 2002; Bushby & Houghton 2005). This complementary approach lends itself more easily to systematic surveys of parameter space, and has had considerable success in qualitatively reproducing solar-like behaviour.

In this paper, we investigate the formation of super-equipartition, localised magnetic features in the quiet Sun. We carry out high resolution numerical simulations of an idealised model of photospheric magnetoconvection. Clearly it is not possible to achieve solar-like values of the viscous and magnetic Reynolds numbers in these simulations (which are both very large at the solar photosphere, see e.g. Ossendrijver 2003). However the Reynolds numbers that are used here are large enough that these simulations (at least qualitatively) reproduce most of the key physical features of flux intensification in photospheric magnetoconvection. The setup of this model and the numerical results that are obtained from it are described in the next two Sections of the paper. In the final part, we discuss the relevance of these results to photospheric magnetic fields and compare our findings with predictions of the simplified ‘‘convective collapse’’ models.

## 2 GOVERNING EQUATIONS AND NUMERICAL METHODS

The model that is considered in this paper is an idealised, local representation of magnetoconvection in the quiet Sun. We solve the equations of three-dimensional compressible magnetohydrodynamics for a plane layer of electrically-conducting, perfect monatomic gas. The layer of gas is heated from below and cooled from above. We assume constant values for the gravitational acceleration  $g$ , the shear viscosity  $\mu$ , the magnetic diffusivity  $\eta$ , the thermal conductivity  $K$ , the magnetic permeability  $\mu_0$  and the specific heat capacities at constant density and pressure ( $c_v$  and  $c_p$  respectively). The axes of the chosen Cartesian frame of reference are oriented so that the  $z$ -axis points vertically downwards (parallel to the gravitational acceleration). Defining  $d$  to be the depth of the convective layer, the gas occupies the region  $0 \leq x, y \leq 4d$  and  $0 \leq z \leq d$ , which gives a wide Cartesian domain with a square horizontal cross-sectional area. Periodic boundary conditions are imposed in each of the horizontal directions. Idealised boundary conditions are imposed at  $z = 0$  and  $z = d$ . These bounding surfaces are held at fixed temperature, and are assumed to be impermeable and stress-free. In addition, any magnetic field that is present is constrained to be vertical at the upper and lower boundaries. Similar models have been considered in several previous studies (see, for example, Matthews et al. 1995; Rucklidge et al. 2000; Weiss et al. 2002; Bushby & Houghton 2005).

It is convenient to formulate the governing equations for magnetoconvection in terms of non-dimensional variables. We adopt non-dimensionalising scalings that are similar to those described by Matthews et al. (1995). All lengths are scaled in terms of the depth of the Cartesian domain,  $d$ , whilst the temperature,  $T$ , and density,  $\rho$ , are both scaled in terms of their values at the upper surface of the domain (which are denoted by  $T_0$  and  $\rho_0$  respectively). Defin-

ing  $R_*$  to be the gas constant, the velocity,  $\mathbf{u}$ , is scaled in terms of the isothermal sound speed at the top of the layer,  $(R_*T_0)^{1/2}$ ; a natural scaling for time is therefore  $d/(R_*T_0)^{1/2}$ , which corresponds to an acoustic timescale. The parameter  $\theta$  denotes the (dimensionless) temperature difference between the upper and lower boundaries. In the absence of any motion the gas is a polytrope with a polytropic index  $m = gd/R_*T_0\theta - 1$ . Rather than relating the magnetic field strength to the Chandrasekhar number (see, for example, Weiss et al. 2002; Bushby & Houghton 2005), we also scale the Alfvén speed at the top of the layer in terms of the sound speed. This implies that the appropriate non-dimensionalising scaling for the magnetic field,  $\mathbf{B}$ , is given by  $(\mu_0\rho_0R_*T_0)^{1/2}$ . Having made these scalings, the governing equations for the density, the momentum density ( $\rho\mathbf{u}$ ), the magnetic field and the temperature are given by

$$\frac{\partial \rho}{\partial t} = -\nabla \cdot (\rho\mathbf{u}), \quad (1)$$

$$\begin{aligned} \frac{\partial}{\partial t} (\rho\mathbf{u}) = & -\nabla (P + |\mathbf{B}|^2/2) + \theta(m+1)\rho\hat{\mathbf{z}} \\ & + \nabla \cdot (\mathbf{B}\mathbf{B} - \rho\mathbf{u}\mathbf{u} + \kappa\sigma\boldsymbol{\tau}), \end{aligned} \quad (2)$$

$$\frac{\partial \mathbf{B}}{\partial t} = \nabla \times (\mathbf{u} \times \mathbf{B} - \kappa\zeta_0\nabla \times \mathbf{B}), \quad \nabla \cdot \mathbf{B} = 0, \quad (3)$$

$$\begin{aligned} \frac{\partial T}{\partial t} = & -\mathbf{u} \cdot \nabla T - (\gamma - 1)T\nabla \cdot \mathbf{u} + \frac{\kappa\gamma}{\rho}\nabla^2 T \\ & + \frac{\kappa(\gamma - 1)}{\rho}(\sigma\tau^2/2 + \zeta_0|\nabla \times \mathbf{B}|^2). \end{aligned} \quad (4)$$

The components of the stress tensor,  $\boldsymbol{\tau}$  are given by

$$\tau_{ij} = \frac{\partial u_i}{\partial x_j} + \frac{\partial u_j}{\partial x_i} - \frac{2}{3}\frac{\partial u_k}{\partial x_k}\delta_{ij}, \quad (5)$$

whilst the pressure,  $P$  is determined by the equation of state for a perfect gas

$$P = \rho T. \quad (6)$$

These governing equations are characterised by several non-dimensional constants, including the Prandtl number,  $\sigma = \mu c_p/K$ , the (non-dimensional) thermal diffusivity,  $\kappa = K/\rho_0 d c_p (R_*T_0)^{1/2}$ , and the ratio of specific heats,  $\gamma = c_p/c_v$ . The ratio of the magnetic diffusivity to the thermal diffusivity,  $\zeta$ , is proportional to the fluid density  $\rho$  (and therefore increases with depth). At the top of the layer  $\zeta = \zeta_0 \equiv \eta\rho_0 c_p/K$ . If all the other parameters are fixed, varying  $\kappa$  is equivalent to varying the mid-layer Rayleigh number,

$$Ra = (m+1 - m\gamma)(1 + \theta/2)^{2m-1} \frac{(m+1)\theta^2}{\kappa^2\gamma\sigma}. \quad (7)$$

This Rayleigh number measures the destabilising effects of a superadiabatic temperature gradient relative to the stabilising effects of diffusion. The parameters are all described in greater detail by Matthews et al. (1995).

The simplest non-trivial equilibrium solution of these governing equations corresponds to a static polytrope with a uniform magnetic field. Initially we restrict attention to the

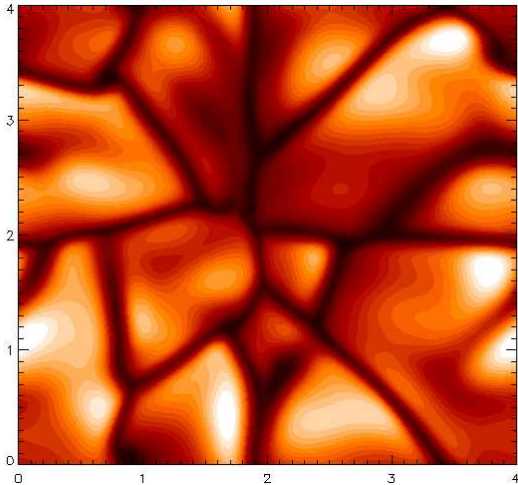


**Figure 1.** The temperature distribution for non-magnetic convection, in a horizontal plane near upper surface of the Cartesian domain. Brighter regions correspond to warmer fluid, cooler areas of fluid are represented by darker regions.

case in which  $\mathbf{B} = 0$ . In this equilibrium solution,  $\mathbf{u} = 0$ ,  $T(z) = 1 + \theta z$  and  $\rho(z) = (1 + \theta z)^m$ . Fixing  $\theta = 10$  and  $m = 1$  gives a highly stratified atmosphere in which the temperature and density both vary by an order of magnitude across the layer. We consider a monatomic gas, therefore  $\gamma = 5/3$ . This implies that the  $m = 1$  polytrope is superadiabatically stratified. For simplicity (and for ease of comparison with previous studies) we set the Prandtl number equal to unity, i.e.  $\sigma = 1$ . A range of values for  $\zeta_0$  is considered in this paper. Finally, the Rayleigh number is chosen to be  $Ra = 4.0 \times 10^5$ . This value for  $Ra$  is more than two orders of magnitude larger than the critical value for the onset of convective instabilities.

The model described above is investigated by carrying out high resolution numerical simulations. For this  $4 \times 4 \times 1$  Cartesian domain, we adopt a computational mesh of  $256 \times 256 \times 160$  grid points. This is a smaller computational domain than that used in some previous studies (see e.g. Bushby & Houghton 2005), and the reduction in box size does influence the global structure of the convective motions by eliminating mesoscale structures (Rucklidge et al. 2000). However, the higher spatial resolution that is used in these calculations enables us to model magnetoconvective behaviour accurately at higher Reynolds numbers, so this is a reasonable compromise (particularly given that the box size probably has little effect upon the localised process of flux concentration). We use a well tested code (see, e.g. Matthews et al. 1995) in which horizontal derivatives are evaluated in Fourier space, whilst vertical derivatives are evaluated using fourth order finite differences. The time-stepping is carried out via an explicit 3rd order Adams-Bashforth scheme, with a variable time-step. The code is efficiently parallelised using MPI, and these simulations have made use of the Cambridge-Cranfield High Performance Computing Facility and the UKMHD Consortium machine based in St Andrews.

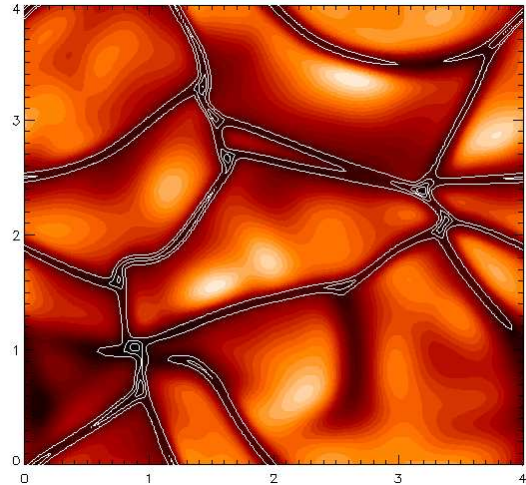


**Figure 2.** The magnetic field distribution during the flux expulsion phase, at  $t = 0.24$ . The shaded contours show the temperature distribution in a horizontal plane just below the upper surface of the computational domain (as described in Fig. 1). The white contours denote constant values of the vertical component of the magnetic field.

### 3 RESULTS

#### 3.1 The initial state

The starting point for these idealised simulations is fully developed non-magnetic convection. In order to generate such a convective state, we consider the equilibrium solution corresponding to a static polytrope with no applied magnetic field, and introduce a small amplitude random temperature perturbation. This convectively-unstable configuration is allowed to evolve until it has relaxed to a statistically steady hydrodynamic state, as illustrated in Fig. 1, which shows a snapshot of the temperature distribution in a horizontal plane just below the upper surface of the computational domain. In this granular pattern, bright regions correspond to broad warm upflows, whilst darker regions correspond to cool narrow downflows. The strength of the convection can be characterised by the mid-layer Reynolds number  $Re = \rho_{\text{mid}} U_{\text{rms}} d / \mu$ , where  $U_{\text{rms}}$  corresponds to the rms-velocity of the convection and  $\rho_{\text{mid}}$  is the density at the mid-layer of the original static polytrope. The Reynolds number here is approximately  $Re = 150$ . As noted in the Introduction, realistic Reynolds numbers for photospheric convection are numerically unobtainable, but the Reynolds number is large enough that instructive results can be obtained in these idealised calculations.

Having established this (purely hydrodynamic) convective state, we then introduce a weak uniform vertical magnetic field,  $B_0 \hat{\mathbf{z}}$ , with  $B_0$  chosen so that the initial magnetic energy is approximately 0.1% of the kinetic energy. A weak imposed field of this form tends to favour the formation of highly localised magnetic features (see, for example, Bushby & Houghton 2005). In what follows, the time at which this magnetic field is introduced is denoted by  $t = 0$ . The subsequent evolution of this magnetic field depends crucially upon the magnetic Reynolds number of the flow,  $Rm = U_{\text{rms}} d / \eta$ . In non-dimensional terms,  $Rm \propto \zeta_0^{-1}$ ; thus it is possible

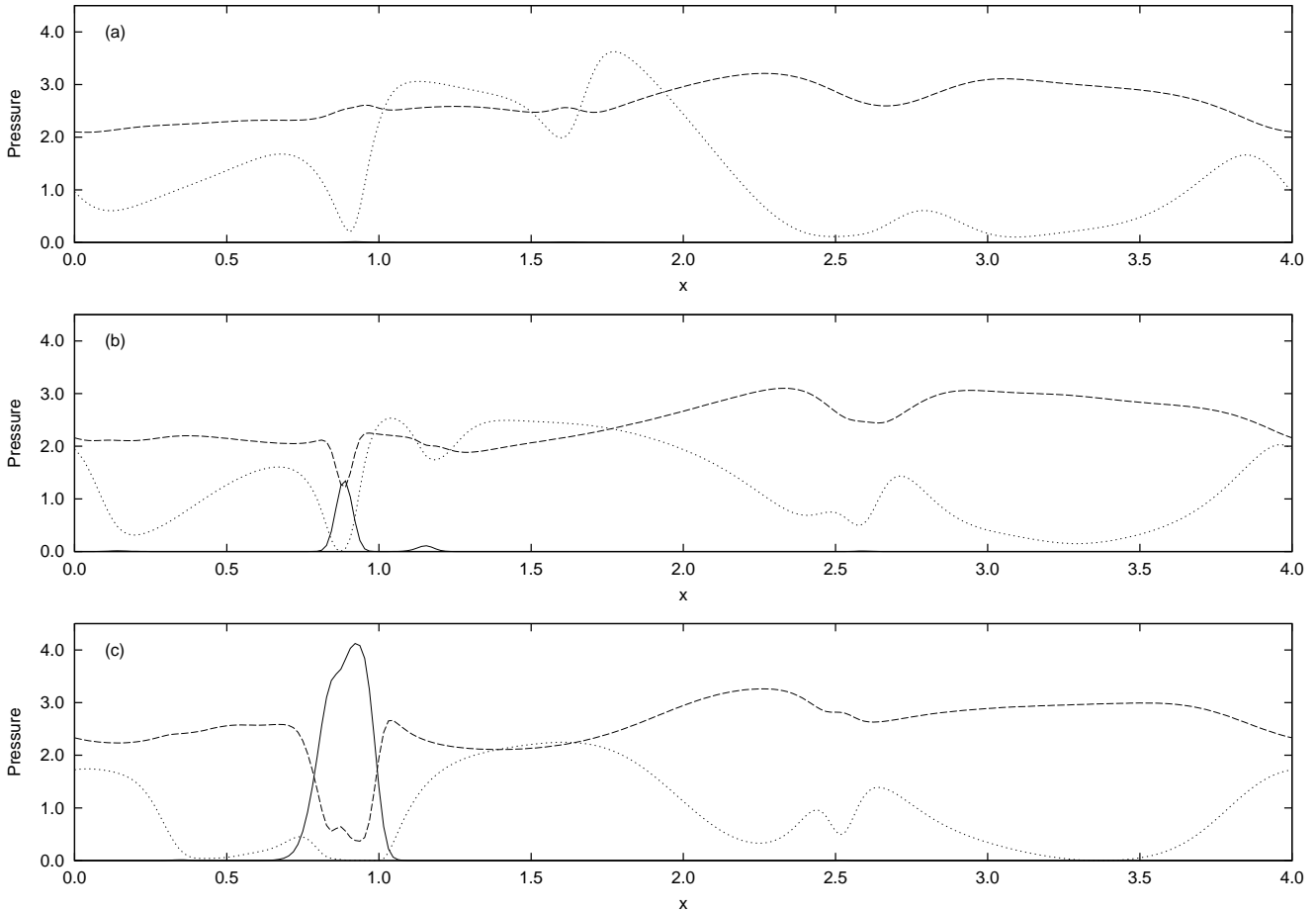


**Figure 3.** The  $x$ -dependence of the pressure distributions (each at fixed  $y$ ) at three different time intervals along a horizontal cut through the strongest magnetic feature at the upper surface. Solid lines correspond to the magnetic pressure,  $P_{\text{mag}}$ ; dashed lines correspond to the gas pressure,  $P_{\text{gas}}$ ; the dotted lines represent the dynamic pressure,  $P_{\text{dyn}}$  (see text). These snapshots are taken at (a)  $t=0.12$ , (b)  $t=0.61$  and (c)  $t=1.61$ .

to investigate a range of values of  $Rm$  simply by repeating the numerical experiment with different values of  $\zeta_0$ . The range investigated is  $0.2 \leq \zeta_0 \leq 2.4$  ( $120 \gtrsim Rm \gtrsim 10$ ). Larger values of  $Rm$  correspond to less diffusive plasmas, and are therefore more relevant to photospheric magnetoconvection, although (as with  $Re$ ) it is not yet possible to carry out fully resolved simulations with realistic values of  $Rm$  for photospheric magnetoconvection. We therefore focus initially upon the case of  $\zeta_0 = 0.2$  ( $Rm \simeq 120$ ). The effects of varying  $\zeta_0$  are discussed later in this Section.

### 3.2 Results for $\zeta_0 = 0.2$

Since the initial magnetic field is comparatively weak, the Lorentz forces play a minor role in the very early stages of evolution in these numerical simulations. During this brief “kinematic” phase, diverging convective motions at the upper surface of the computational domain rapidly expel magnetic flux from the granular interiors. This process causes magnetic flux to accumulate in the convective downflows in the intergranular lanes. The strongest field concentrations tend to occur at the vertices between neighbouring granules, due to the fact that any flows along the intergranu-

lar lanes tend to converge upon these vertices. The process of flux expulsion and accumulation is illustrated in Fig. 2, which shows the distribution of the vertical component of the magnetic field during this flux expulsion phase. In this (relatively) high  $Rm$  regime, the width of the localised magnetic features is comparable to the width of the narrow intergranular lanes.

As these localised concentrations of magnetic flux form, the principle of flux conservation implies that the magnetic energy density in these regions rapidly increases to the point where the Lorentz forces become dynamically significant. In the upper layers of the computational domain, most of the magnetic energy resides in the vertical component of the magnetic field, and the horizontal gradients in this field component are usually much larger than any variations in the vertical direction. This implies that the horizontal magnetic pressure gradient (i.e. the horizontal component of  $\nabla [\mathbf{B}^2/2\mu_0]$ ) is the dominant component of the Lorentz force. The effects of the magnetic pressure are most apparent near the surface, where the gas pressure is relatively small. The magnetic pressure gradient tends to inhibit the converging convective motions that are responsible for driving the flux concentration process. However, the

flux amplification process is not immediately suppressed, because the total (i.e. gas plus magnetic) pressure increases more gradually than the magnetic pressure alone. This is due to the fact that the local convective downflows rapidly carry fluid away from the surface regions of the magnetic feature. These downflows are responsible for partially evacuating the upper regions of the magnetic features, which in turn leads to a reduction in the local gas pressure. This reduction in gas pressure (at least partially) compensates for the increased magnetic pressure. In the most intense magnetic flux concentrations, the gas pressure drops to as little as a few percent of its initial value at the surface before the magnetic field becomes locally strong enough to suppress the vertical convective motions. A combination of the suppression of these vertical motions plus the effects of diffusion eventually halts this flux concentration process.

To describe this process in a more quantitative fashion, it is useful not only to consider the variations of the gas pressure ( $P_{\text{gas}}$ ) and the magnetic pressure ( $P_{\text{mag}}$ ), but also the dynamic pressure ( $P_{\text{dyn}}$ ), which represents the dynamical influence of the convective motions. Following Hurlburt & Toomre (1988), we define  $P_{\text{dyn}} = \rho|\mathbf{u}|^2$  (although note that other definitions have been used in some other studies, e.g., Weiss et al. 1996). Whilst this expression does not correspond directly to a pressure term in the momentum equation (2), it does usefully quantify the vigour of the convective motions. Since the mean Mach number at the surface is typically in the region of 0.5 (the peak value is usually close to unity), we would expect  $P_{\text{dyn}}$  to play a significant dynamical role. Fig. 3 illustrates the time-evolution of these pressure distributions immediately after the magnetic field is introduced. To generate a one-dimensional pressure map, we fix the value of  $y$  so that a horizontal cut (in the  $x$  direction) along the upper surface of the computational domain passes through the strongest magnetic feature. The three plots in Fig. 3 show the surface pressure distributions along such a cut at three different times. These plots clearly illustrate the scenario that was described in the previous paragraph. As the magnetic pressure grows, there is a corresponding decrease in the gas pressure as fluid rapidly drains out of the surface regions of the magnetic feature. Once the feature has formed (lower plot of Fig. 3), convective motions are strongly suppressed and the gas pressure in the magnetic region is very much smaller than that of the surrounding field-free fluid. Although partial evacuation, with accompanying field intensification, has already been observed in several previous studies (e.g. Hurlburt & Toomre 1988; Weiss et al. 1996; Vögler et al. 2005), the level of evacuation is much more dramatic in these simulations.

The most surprising aspect of Fig. 3 is the fact that the magnetic pressure within the final localised flux concentration is much larger than the gas pressure of the surrounding non-magnetic fluid. The formation of such an ultra-intense (predominantly vertical) magnetic flux concentration implies that, in the absence of magnetic curvature effects, the surrounding convective motions must be playing an active role in the confinement of this magnetic feature. The significance of the dynamic pressure is illustrated in Fig. 3 – it is clear that the dynamic pressure around the magnetic feature can often be comparable to the local gas pressure. This shows that the dynamical influence of the surrounding convective motions cannot be ignored when considering models

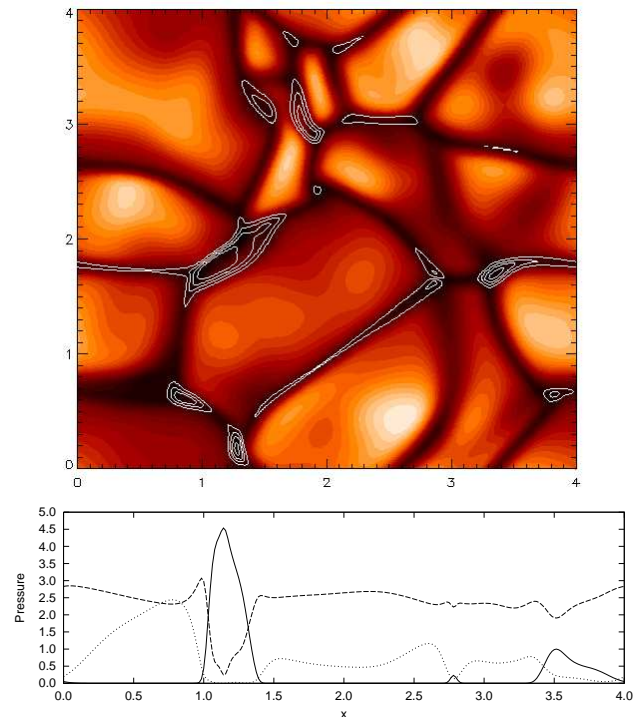


**Figure 4.** The magnetic field distribution at  $t = 26.26$  (after several convective turnover times). Top: Like Fig. 2, this shows contours of the vertical magnetic field component superimposed upon the temperature profile near the upper surface of the computational domain. Bottom: The pressure distributions along a horizontal cut through the strongest magnetic feature at the surface. As in Fig. 3, the solid line corresponds to the magnetic pressure, the dashed line corresponds to the gas pressure, whilst the dynamic pressure is represented by a dotted line.

of photospheric magnetic field intensification. It should also be stressed that the magnetic energy density of the flux concentration that is illustrated in Fig. 3 is much larger than the mean kinetic energy density (i.e.  $P_{\text{dyn}}/2$ ) of the surrounding granular convection. These simulations provide confirmation of the fact that the process of partial evacuation is important in the production of such super-equipartition fields. Without such a reduction in the local gas pressure, it is difficult to see how convective motions alone could produce such a strong magnetic feature.

All the discussion so far has focused upon the early stages of these numerical simulations. The process of magnetic field intensification is arguably the most interesting phase of the dynamics, although the evolution of the resulting magnetic features also raises important issues. In the present idealised model, the net imposed vertical magnetic flux is a conserved quantity, so there will always be some accumulations of vertical magnetic flux somewhere within the computational domain. However, what is less clear is whether or not the occurrence of super-equipartition magnetic fields is a transient feature of the model. Fig. 4 shows the magnetic field distribution several convective turnover times after the magnetic field was first introduced. It is clear that the most intense flux concentrations are still partially evacuated, and it is also clear that the magnetic energy

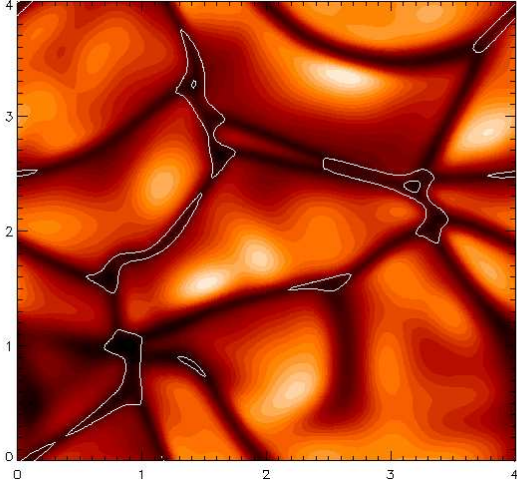


**Figure 5.** The magnetic flux distribution during the kinematic phase for  $\zeta_0 = 1.2$ . Like Fig. 2, this plot is a snapshot of the upper surface of the computational domain at  $t = 0.24$  and shows the spatial variation of the temperature and the vertical magnetic field component. For ease of comparison, the same scales have been used in Fig. 2 and Fig. 5 for both the magnetic field and the temperature.

density of these regions still exceeds the mean kinetic energy density of the surrounding convection. In addition, the fact that the internal magnetic pressure is still much larger than the external gas pressure indicates that the surrounding convective motions are still playing a key role in the confinement of the magnetic feature. During their evolution, these features continuously interact with the convective motions, which implies that they are deformed, shredded and advected around the domain in a time-dependent fashion. However, despite these complex interactions, ultra-intense super-equipartition magnetic features seem to be a robust feature of the simulation and are not simply a transient phenomenon.

### 3.3 The effects of varying $\zeta_0$

One of the key parameters in these simulations is the magnetic Reynolds number,  $Rm$ . Computational restrictions limit the range of values of  $Rm$  that can be considered, and all values that can be simulated will be very much smaller than real photospheric values. However, the simulation that has already been described qualitatively illustrates some of the main physical processes that occur during photospheric magnetic flux amplification. In this Section, we assess the effects of repeating this simulation for different values of  $\zeta_0$ . This is equivalent to varying the magnetic Reynolds number of the flow, which is inversely proportional to  $\zeta_0$ : smaller values of  $Rm$  correspond to larger values of  $\zeta_0$  and vice-versa. In order that comparisons can easily be made between the different cases, all magnetohydrodynamical simulations are started from exactly the same hydrodynamic initial conditions.

Even during the brief kinematic phase, clear trends are observed as the parameter  $\zeta_0$  is varied. The effects of some of these trends are illustrated in Fig. 5, for  $\zeta_0 = 1.2$ . Like Fig. 2,

**Table 1.** The  $\zeta_0$ -dependence of the magnitude of the vertical magnetic field component at a fixed position at the upper surface of the computational domain. The time is fixed at  $t = 0.12$ , and the centre of the magnetic feature is at  $(x, y) = (3.16, 2.39)$  in all cases. Magnetic field strengths are normalised in terms of the strength of the imposed magnetic field

| $\zeta_0$ | $B_z(max)/B_z(initial)$ |
|-----------|-------------------------|
| 0.2       | 3.61                    |
| 0.3       | 3.50                    |
| 0.4       | 3.40                    |
| 0.6       | 3.23                    |
| 1.2       | 2.85                    |
| 2.4       | 2.42                    |

this shows the spatial distribution of the temperature and the vertical component of the magnetic field at the upper surface of the computational domain. In order to allow direct comparison between Fig. 2 and Fig. 5, this snapshot of the simulation is also taken at  $t = 0.24$ , and the contours are plotted at the same levels – this implies that the scales for temperature and magnetic field correspond directly to those used in Fig. 2. In this kinematic phase, the temperature field is the same in both plots, however it is immediately apparent that the magnetic field structures in Fig. 5 are weaker and less localised than those seen in the  $\zeta_0 = 0.2$  case. This is a consequence of the increased importance of diffusion for larger values of  $\zeta_0$  (equivalently, lower values of  $Rm$ ). The influence that  $\zeta_0$  has upon the magnetic field in this kinematic phase is quantified in Table 1. Here, we measure the strength of the vertical component of the magnetic field at  $(x, y, z) = (3.16, 2.39, 0)$  and  $t = 0.12$ , as a function of  $\zeta_0$ . This spatial location corresponds to the centre of the strongest surface magnetic feature at  $t = 0.12$ , which does not depend upon  $\zeta_0$  in the kinematic regime (although the location of this peak field is obviously a function of time). The table confirms that, at a fixed time, there are weaker fields at lower values of  $Rm$ . For simple flows, it is possible to construct a similarity solution for this kind of kinematic flux concentration, which leads to a power-law relationship between the peak magnetic field and the magnetic Reynolds number (see, e.g., Proctor & Weiss, 1982). Unfortunately, due to the complexity of the flow patterns in this case, there appears to be no analogous scaling here.

For  $\zeta_0 = 0.2$ , it was found that the high magnetic pressure in the strongest magnetic field concentrations quickly led to the partial evacuation of these magnetic features. Since these magnetic flux concentrations grow more gradually for larger values of  $\zeta_0$ , this partial evacuation process is much slower in these cases and the effects of diffusion tend to play a more dominant role in limiting the flux concentration. Therefore, the amount of evacuation that occurs decreases with increasing  $\zeta_0$ . This demonstrates that the rapid intensification that occurred in the  $\zeta_0 = 0.2$  case is very much a high magnetic Reynolds number phenomenon. However, some evacuation is observed in all cases that were investigated except  $\zeta_0 = 2.4$ , and wherever features do become partially evacuated, super-equipartition magnetic features are observed. Fig. 6 shows time-averaged probability density functions (pdfs) for the vertical component of the surface magnetic field, for three different values of  $\zeta_0$ . In all cases,

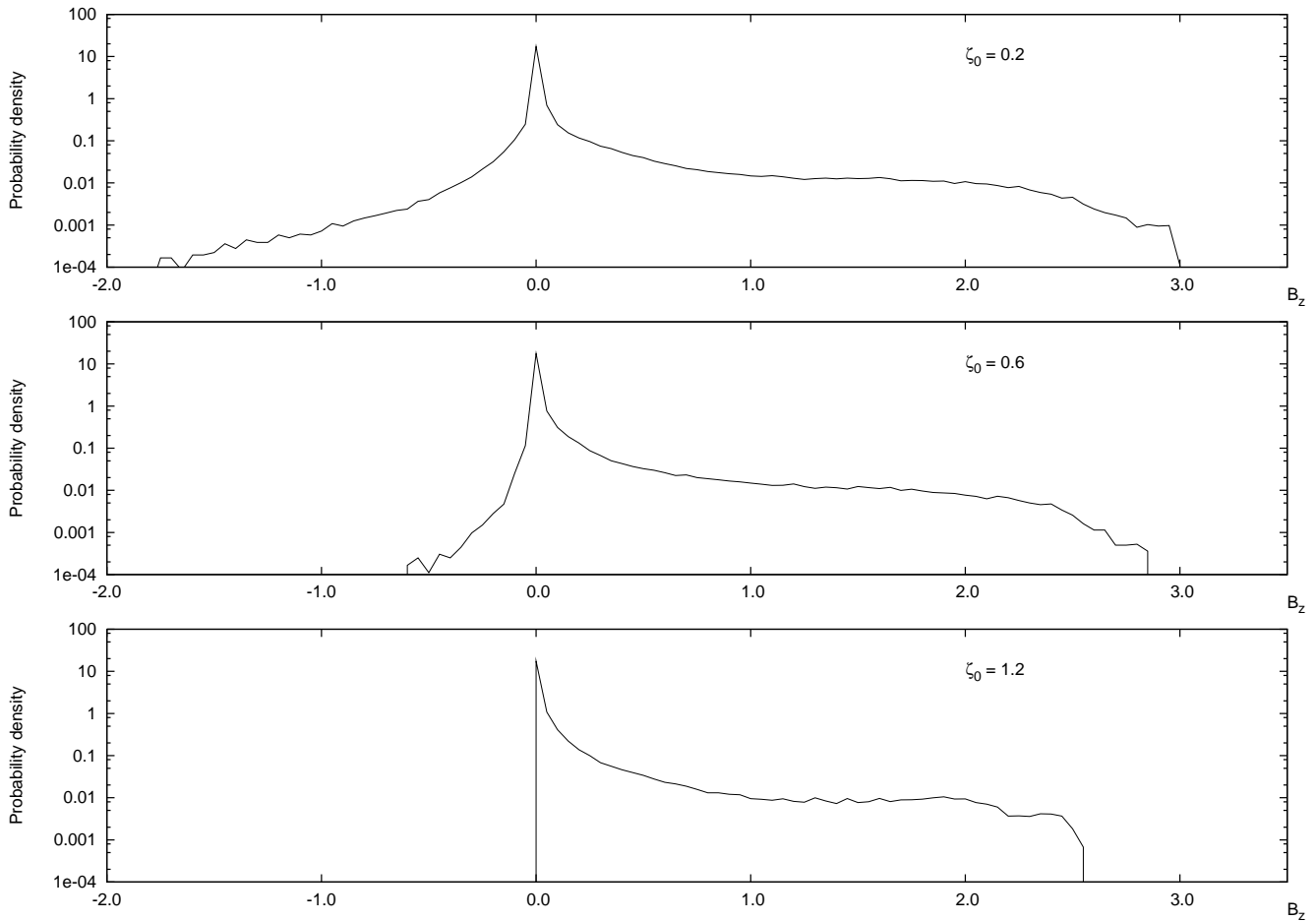


**Figure 6.** Probability density functions for the vertical component of the magnetic field at the upper surface of the computational domain. These functions correspond to different values of  $\zeta_0$ . These values are  $\zeta_0 = 0.2$  (top),  $\zeta_0 = 0.6$  (middle) and  $\zeta_0 = 1.2$  (bottom). For smaller values of  $\zeta_0$  (or, equivalently, larger values of  $Rm$ ) there is a higher probability of stronger fields and there is a greater proportion of reversed polarity magnetic flux.

the pdfs peak at  $B_z = 0$ , which implies that the majority of the domain is field-free. In addition, there is a significant component of reversed magnetic flux at lower values of  $\zeta_0$ . At higher  $Rm$  there is a greater tendency for flux to be advected with any fluid flow, and these convective motions certainly have the potential to reverse magnetic flux at the granular boundaries at the surface of the domain. Most interestingly, there is not a large difference between the peak fields in the pdfs for  $\zeta_0 = 0.6$  and  $\zeta_0 = 0.2$ . Equivalently, the magnitude of the peak field appears to be only weakly dependent upon  $Rm$  in this particular parameter regime. This suggests that rather than being controlled by diffusive effects, the peak attainable magnetic field in this parameter regime is determined by the combined effects of the external gas and dynamic pressures. So, although ultra-intense magnetic features form more rapidly at higher  $Rm$ , these features can also be produced at lower values of  $Rm$ , provided that magnetic diffusion does not completely inhibit the flux concentration process before the magnetic field can become dynamically active.

#### 4 CONCLUSIONS

This paper describes results from a series of high resolution numerical experiments that were designed to investigate the formation of localised magnetic flux concentrations at the solar photosphere. By adopting an idealised model, it was possible to assess the effects that varying the magnetic Reynolds number might have upon this flux intensification process. As expected, magnetic flux tends to accumulate preferentially in convective downflows, where it forms localised features – the horizontal scale of these features decreases with increasing magnetic Reynolds number. High magnetic pressures lead to the partial evacuation of these features as they form. At high values of  $Rm$ , the resulting field strengths are typically much larger than the equipartition value at which the local magnetic energy density balances the mean kinetic energy density of the surrounding granular convection. In addition, the strongest magnetic fields that are obtained exert a magnetic pressure that is significantly larger than the external gas pressure. The appearance of these ultra-intense magnetic fields shows that the dynamic pressure that is associated with the surrounding convection must be playing a key role in the confinement of these magnetic features to localised regions. Some super-equipartition magnetic fields

are found in all cases except the most diffusive case (corresponding to  $\zeta_0 = 2.4$ ).

It is interesting to relate these results to convective collapse models (see, e.g., Webb & Roberts 1978; Spruit & Zweibel 1979). Although those models are certainly an idealised representation of photospheric magnetic field intensification, our simulations suggest that they correctly identify the most important process in the formation of super-equipartition magnetic fields, namely the partial evacuation of magnetic regions by convective downflows. Our simulations do, however, raise some important issues relating to convective collapse. First, convective collapse models typically adopt an initial condition that corresponds to a thin flux tube embedded in a static atmosphere. Since such magnetic features form in well-established convective downflows, this static equilibrium never occurs in our simulations. Additionally, the evacuation process seems to begin before the flux accumulation process finishes. So our simulations could be seen as describing an “adjustment” rather than an instability. The second point that is raised by these simulations concerns the pressure balance. Convective collapse models assume a constant balance between the external gas pressure and the gas and magnetic pressures within the flux tube. Our simulations indicate that the dynamical effects of the surrounding convection are playing a significant role in the confinement of these magnetic features. The neglect of this dynamic pressure underestimates the strength of the strongest magnetic fields that can be generated. Finally, Cameron & Galloway (2005) have modelled aspects of convective collapse by conducting numerical simulations of laminar magnetoconvection in a simplified geometry. From these simulations they argue that super-equipartition magnetic features must be structured on a kinematic scale at the solar photosphere. Although only a limited range of values for  $Rm$  has been considered here, our simulations do produce some super-equipartition fields on larger scales, and so contradict their view.

Put differently, where the flow converges on an intense flux concentration there has to be an excess stagnation pressure. Here this is provided by the magnetic field in a region where the gas pressure is reduced. This is in total contrast with the simulation of umbral convection by Schüssler and Vögler (2006), where a divergent rising plume is associated with a weaker field, and the excess pressure results from an enhancement of density (associated with buoyancy braking) instead.

When comparing results from these simulations with photospheric observations, it is important to remember some of the simplifying assumptions in this model. Processes such as radiative transfer have been neglected, so it is not possible to make detailed spectral comparisons between these simulations and observations. Nevertheless, this idealised approach has had a great deal of success in reproducing qualitative features of photospheric magnetoconvection. In qualitative terms, our simulations appear to be consistent with solar observations and provide a plausible explanation for the observation of super-equipartition magnetic features in the intergranular lanes in the quiet Sun. However, this model does have other limitations, notably the fact that many of the parameters that are used are not closely related to realistic solar values. Another limitation that should be noted is the fact that (due to the periodic boundary conditions) the

imposed magnetic flux is independent of both  $z$  and  $t$ . This implies that net vertical magnetic flux cannot enter or leave the domain, therefore the initial non-zero magnetic flux is an invariant quantity in the model. In the quiet Sun, there is a continuous emergence of mixed polarity magnetic flux, which will interact with existing magnetic features. Such interactions will tend to limit the lifetimes of these magnetic features. This is something that cannot be represented in our idealised simulations, though it may be possible to make progress by careful choice of initial conditions.

In the Introduction, we noted that it is still not clear whether quiet Sun magnetic features are simply fragments of reprocessed magnetic flux or whether they are generated locally as the result of small-scale dynamo action. In fact, this model of compressible convection can drive a small-scale dynamo once the magnetic Reynolds number exceeds a threshold of about  $Rm = 250$ . However, even for a marginally-excited dynamo, the magnetic Prandtl number is of order 2 which is very much larger than the magnetic Prandtl number in the solar photosphere. Whether or not such a dynamo could operate in the low magnetic Prandtl number regime has been the subject of considerable debate (see, for example, Boldyrev & Cattaneo 2004; Schekochihin et al. 2005). Although our idealised simulations do assume some pre-existing magnetic field (i.e. they do not generate this field self-consistently), the processes of magnetic flux expulsion and intensification that are illustrated by these simulations are generic and are therefore likely to be of relevance to the solar photosphere whether or not a local dynamo is operating.

This work is motivated by high resolution observations of the solar photosphere. Although current ground-based instruments, such as the Swedish 1-metre Solar Telescope, are already provided very detailed images of the photosphere, it is likely that newer instruments (including those carried on the recently launched Hinode satellite) will reveal many new features of photospheric magnetoconvection. Over the next few years, these new observations will enable us to refine our current theoretical models, but will also inevitably present new theoretical challenges.

## ACKNOWLEDGEMENTS

This work was supported by PPARC/STFC while PJB held a postdoctoral appointment at DAMTP in Cambridge. The numerical simulations that were described in this paper made use of computing facilities belonging to the UKMHD Consortium (based at the University of St Andrews) and the Cambridge-Cranfield High Performance Computing Facility.

## REFERENCES

- Berger T. E. et al., 2004, *A&A*, 428, 613
- Berger T. E., Title A. M., 1996, *ApJ*, 463, 365
- Berger T. E., Title A. M., 2001, *ApJ*, 553, 449
- Boldyrev S., Cattaneo F., 2004, *Phys. Rev. Lett.*, 92, 144501
- Bushby P. J., Houghton S. M., 2005, *MNRAS*, 362, 313
- Cameron R., Galloway D., 2005, *MNRAS*, 358, 1025
- Cattaneo F., 1999, *ApJ*, 515, L39
- Cattaneo F., Hughes D. W., 2006, *JFM*, 553, 401

- Centeno R. et al., 2007, ApJ, 666, L137
- Domínguez Cerdeña I., Kneer F., Sánchez Almeida J., 2003, ApJ, 582, 55
- Domínguez Cerdeña I., Sánchez Almeida J., Kneer F., 2006, ApJ, 636, 496
- Galloway D. J., Proctor M. R. E., Weiss N. O., 1977, Nature, 266, 686
- Galloway D. J., Proctor M. R. E., Weiss N. O., 1978, JFM, 87
- Galloway D. J., Moore D. R., 1979, Geophys. Astrophys. Fluid Dyn., 12, 73
- Grossmann-Doerth U., Keller C. U., Schüssler M., 1996, A&A, 315, 610
- Grossmann-Doerth U., Schüssler M., Steiner O., 1998, A&A, 337, 928
- Hughes D. W., Proctor M. R. E., 1988, Ann. Rev. Fluid Mech., 20, 187
- Hurlburt N. E., Toomre J., 1988, ApJ, 327, 920
- Kerswell R., Childress S., 1992, ApJ, 385, 746
- Khomenko E. V., Shelyag S., Solanki S. K., Vögler A., 2005, A&A, 442, 1059
- Lin H., Rimmele T., 1999, ApJ, 514, 448
- Matthews P. C., Proctor M. R. E., Weiss N. O., 1995, JFM, 300, 287
- Ossendrijver M., 2003, A&ARv, 11, 287
- Proctor M. R. E., Weiss N. O., 1982, Rep. Prog. Phys., 45, 1317
- Proctor M. R. E., 1983, in Stenflo J. O. ed, Proc. IAU Symp. 102, Solar and stellar magnetic fields: Origins and coronal effects. Dordrecht, D. Reidel Publishing Co., p301
- Proctor M. R. E., Weiss N. O., 1984, in Proc. of the Fourth European Meeting on Solar Physics, The Hydromagnetics of the Sun, p77
- Rezaei R., Steiner O., Wedemeyer-Böhm S., Schlichenmaier, R., Schmidt W., Lites B. W., 2007, A&A, in press
- Rucklidge A. M., Weiss N. O., Brownjohn D. P., Matthews P. C., Proctor M. R. E., 2000, JFM, 419, 283
- Sánchez Almeida J., 2007, ApJ, 657, 1150
- Scharmer G. B., Gudiksen B. V., Kiselman, D., Löfdahl M. G., Rouppe van der Voort, L. H. M., 2002, Nature, 420, 151
- Schekochihin A. A., Haugen N. E. L., Brandenburg A., Cowley S. C., Maron J. L., McWilliams J. C., 2005, ApJ, 625, L115
- Schüssler M., Vögler A., 2006, ApJ, 641, L73
- Spruit H. C., 1979, SoPh, 61, 363
- Spruit H. C., Zweibel, E. G., 1979, SoPh, 62, 15
- Stein R. F., Nordlund Å., 2006, ApJ, 642, 1246
- Unno W., Ando H., 1979, GApFD, 12, 107
- Thomas J. H., Weiss N. O., 1992, in *Sunspots: Theory and Observations*, ed. J. H. Thomas & N. O. Weiss (Dordrecht: Kluwer), p. 3
- Thomas J. H., Weiss N. O., 2008, *Sunspots and Starspots* (Cambridge: Cambridge University Press), in press.
- Vögler A., Schüssler M., 2007, A&A, 465, L43
- Voegler A., Shelyag S., Schüssler M., Cattaneo F., Emonet T., Linde T., 2005, A&A, 429, 335
- Webb A. R., Roberts B., 1978, SoPh, 59, 249
- Weiss N. O., Brownjohn D. P., Matthews P. C., Proctor M. R. E., Brownjohn D. P., 1996, MNRAS, 283, 1153
- Weiss N. O., Proctor M. R. E., Brownjohn D. P., 2002, MNRAS, 337, 293

This paper has been typeset from a  $\text{\TeX}$ / $\text{\LaTeX}$  file prepared by the author.